Electron-beam-induced deposition of platinum at low landing energies

A. Botman[a)]
Faculty of Applied Sciences, Delft University of Technology, Lorentzweg 1, 2628 CJ Delft, The Netherlands

D. A. M. de Winter
Utrecht University, H. R. Kruyt Building, Padualaan 8, 3584 CH Utrecht, The Netherlands

J. J. L. Mulders
FEI Electron Optics, Achtseweg Noord 5, 5600 KA Eindhoven, The Netherlands

(Received 18 June 2008; accepted 28 July 2008; published 1 December 2008)

Electron-beam-induced deposition of platinum from methylcyclopentadienyl-platinum-trimethyl was performed with a focused electron beam at low landing energies, down to 10 eV. The deposition growth rate is maximal at 140 eV, with the process being over ten times more efficient than at 20 kV. No significant dependence of composition with landing energy was found in the deposits performed at energies between 40 and 1000 eV. This study provides further evidence for the dissociation process being primarily driven by the sub-20-eV secondary electrons.
 [DOI: 10.1116/1.2976576]

I. INTRODUCTION

Electron-beam-induced deposition[1,2] (EBID) is a promising technique for nanoscale rapid prototyping and nanolithography.[3] EBID in its simplest form, directed carbon contamination growth, was first described in 1976,[4] but the exact mechanism of the precursor dissociation process is still not yet well understood. At the heart of the question is the total adsorbed precursor electron-impact deposition cross section, which is not known for these compounds in these conditions,[5] although increasingly educated guesses are being made and used.[6,7] (This total *deposition* cross section is the sum of the individual *dissociation* cross sections from each fragment of the original precursor molecule. The sum is weighted with the probability that each fragment remains to form a deposit rather than desorbed. From here onwards we simply refer to this as the "dissociation cross section," for simplicity.) Some authors believe that the cross-section peaks for low-energy secondary electrons,[5] whereas others argue that high-energy dissociation events are underestimated and that primary electrons, backscattered electrons (BSEs), and fast secondary electrons also contribute "significantly" to EBID growth.[1,8,9] Better understanding of the physics of this dissociation process will allow us to attain better control of the size, shape, and quality of the depositions.

To obtain insight into this decomposition cross section, it is useful to obtain data on the yield of deposition as a function of electron beam energy. To date there have been some studies on this subject at the standard energies used in scanning microscopes ranging from 1 to 30 keV.[9–11] However it is experimentally difficult to go lower than 1 keV with a focused beam in a standard scanning electron microscope (SEM) and to date there exists no relevant literature on the low-energy part of the curve, except for Hoyle *et al.*[12] for tungsten from $W(CO)_6$ and Kunz and Mayer[13] for the growth and etching of SiO_x.

This study reports on the yield at electron landing energies over the full range from 10 eV up to 20 keV using a retarding field arrangement and a frequently used standard platinum precursor [methyl cyclopentadienyl-platinum-trimethyl ($MeCpPtMe_3$)].

II. EXPERIMENT

A FEI Nova 600 DualBeam system (combining a focused ion beam microscope and a scanning electron microscope in one instrument) was used for deposition. This system was equipped with standard gas injectors (GIS) enabling beam-induced depositions with either ions or electrons. All our depositions were performed using the electron beam, with the beam parameters as given below. The platinum precursor was methylcyclopentadienyl-platinum-trimethyl $MeCpPtMe_3$ (CAS: 94442-22-5). The base chamber pressure prior to deposition was better than 2×10^{-6} mbar, this value changed to around 2×10^{-5} mbar during deposition.

The sample stub was electrically isolated from the sample stage, and a shielded wire leading to a feedthruogh was arranged such that the stub could be held at a potential of choice with respect to the SEM final lens and stage that are held at ground potential. The sample was silicon with a large area of 2×3 cm^2 such that the retarding field setup between the sample and the final lens would be as uniform and vertical as possible, locally along the electron beam path. The sample to final lens distance was 5 mm and the depositions were made at the center of the sample. For the same reason the standard GIS needle (normally at ground potential) was exchanged for one that was shorter so that it did not protrude below the final lens level. The entire arrangement within the SEM chamber is shown in Fig. 1. Outside the chamber a voltage source was connected to the feedthrough, and an accurate voltmeter was added to the circuit. By varying the

[a)]Author to whom correspondence should be addressed; electronic mail: a.p.j.m.botman@tudelft.nl

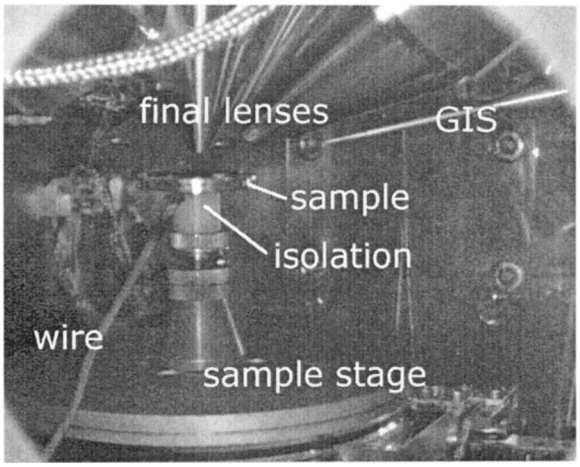

FIG. 1. Image of microscope chamber showing sample stage, isolated sample stub, wire for biasing the stub, final lenses (electron and ion columns), and GIS needle.

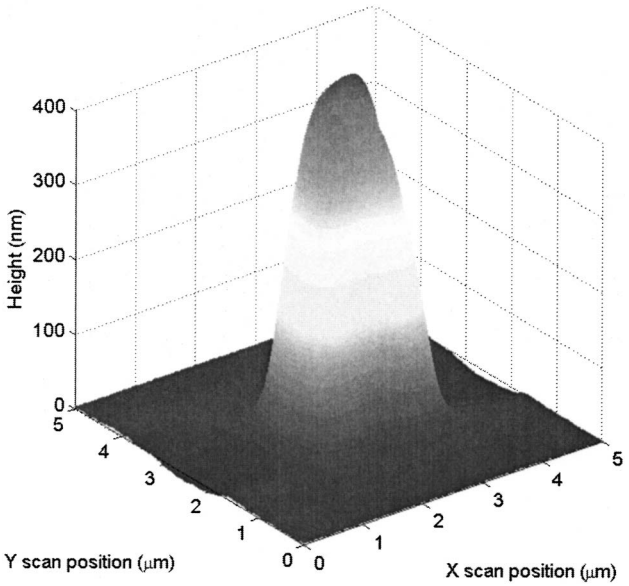

FIG. 2. AFM scan of a successful deposition at 80 eV.

voltage on the voltage source it was therefore possible to vary the landing energy of the electrons focused on the sample.

The substrate was a silicon wafer piece with a layer of native oxide. This native oxide was removed by ion beam milling (30 keV, 0.28 nA, 15×15 μm^2 for 54 s) once the sample was in the SEM vacuum, since at very low energies a substantial part of the electron beam is deposited in the oxide layer, resulting in too much sample charging and therefore time-dependent image drift. A vacuum-compatible silver-paint dot (giving well-defined high-contrast features at many length scales) was present on the substrate at a reference position, to enable checking of the focus and stigmation settings at various moments. All SEM detectors, normally biased to collect the image-forming secondary electrons, were set to zero biasing while the retarding field was present, to prevent them from affecting the low-energy electrons. The beam currents were calibrated by a Faraday cup and picoammeter at zero bias. The repeatability of beam current setting is better than 1%.

Depositions above 1 keV were performed with the beam at the desired landing energy with no sample bias. For depositions below 1 keV, the beam energy at the exit of the pole piece was 1 keV and the bias was set between 0 and −1 kV. Beyond −1 kV biasing, the image observed was that of the final lens rather than of the sample, which meant that the substrate had become perfectly reflective to electrons. The point at which this reversal took place was taken to be 0 eV landing energy, this was determined to ±1 V. Therefore, for instance, according to this retarding field configuration, a sample bias of −980 V gave us an effective electron landing energy of 20 eV at the sample. It was verified that (for instance) the deposition yield performed at 1 keV with 0 V bias was identical to that performed at 1.5 keV with −500 V bias.

The target deposit geometry was a cube, with a base of nominally 500×500 nm^2, patterned in a serpentine manner. The dwell time per pixel was 200 ns, the distance between pixels was 40 nm, and the overlap parameter was 0%. The total deposition time for one structure was 10 min.

Once the depositions were completed the samples were subsequently stored in air. AFM analysis was performed to obtain the volume of each deposit. Subsequently the composition of the samples was analyzed using low-kV EDX. Since the deposits were small in volume, the composition data were thereafter corrected using the thin-film $\varphi(\rho z)$ curve from Pouchou and Pichoir.[14]

III. RESULTS

The results are expressed as a volumetric yield per electron present in the primary beam. This accounted for the beam current variations as a function of beam energy above 1 kV, an inherent characteristic of the instrument.

An example deposit is shown in Fig. 2 in the form of an AFM scan. The deposit yield results are shown in Fig. 3. The structure deposited at 10 eV was too small to be located for AFM measurement, hence is not shown. The main contribution to the error bars arises from the determination of the deposit's volume from the AFM height maps. The yield is maximum at 140 eV. At this energy the dissociation process efficiency is over ten times that at 20 keV. The results for the depositions in the conventional 1–20 keV range are consistent with those reported in the literature.[9–11]

Using this data, the EBID rate equation given by Allen *et al.*,[15] and assuming a form for the electron-impact dissociation cross section for the adsorbed precursor, we can calculate the expected deposition yield. (The electron fluxes used in the calculation origin from a Monte Carlo model, the details of which will be published shortly by other authors. It is important to note that we count both electrons going into and coming out of the substrate hence the BSE yields used are higher by the amount of electrons used in the primary beam.) By comparing to our measured yield we can then verify the

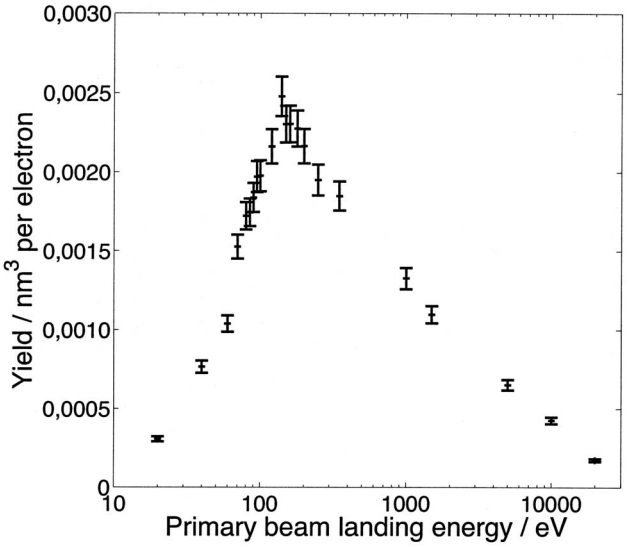

FIG. 3. Deposition yield (nm^3 per electron in the primary beam) as a function of beam landing energy (eV).

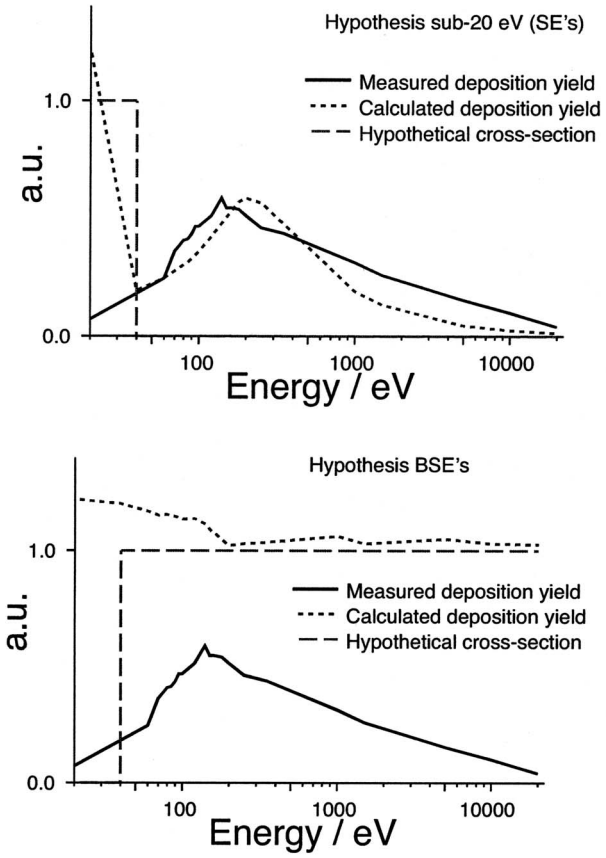

FIG. 4. Two hypotheses as to the possible cross-section form. Top: calculation of what deposition yield would be obtained, assuming a cross section being nonzero for the sub-20-eV electrons (SEs) and zero everywhere else. The form of the calculated yield [obtained by convoluting with the electron fluxes at each electron energy for each landing energy according to the EBID growth equation given in Allen *et al.* (Ref. 16)] fits well with the measured one except below 20 eV. Bottom: same as top, assuming a cross section that is only nonzero for the backscattered and primary electrons. The fit to the measured data is less good for this hypothesis. This indicates that the sub-20-eV plays an important role in the dissociation process.

accuracy of the assumed cross-section form. In Fig. 4 we propose two different hypotheses for the cross section: that either the sub-20-eV electrons are mostly responsible for the dissociation process (top Fig. 4), or that the backscattered and primary electrons are (bottom Fig. 4). It can be observed that the former assumption gives the better fit.

Between 40 and 1000 eV, the elemental composition of the deposits does not vary significantly with landing energy (Fig. 5). The atomic concentration of platinum is evenly scattered between 14 and 22 at. %. This means that the depositions performed at low landing energy are equivalent to those performed at the more standard beam energies (e.g., 20 kV).

IV. DISCUSSION

There are two limitations inherent in this particular experiment. First, the image magnification changes with the retarding field magnitude due to the lens action between the final lens and sample. The electron dose at 1 kV was 1.3 times lower than at the minimum energy of 10 eV. In this experiment we have not corrected for this effect, although it is expected to be minor. Second, we compare directly depositions done with a retarding field configuration (below 1 kV) and without (above 1 kV). Some checks were implemented to ensure that this was valid (as described above) and we are confident that a direct comparison is indeed allowed.

Imaging at the low landing energies yielded the expected contrast variations; for instance an image contrast reversal was observed around 40 eV.[16] It became increasingly difficult to focus and stigmate the beam at the lower landing energies, although this was still possible at 20 eV and 50.000× magnification, and with quite some effort even at 10 eV. At very low landing energies it is expected that the probe profile broadens significantly at the substrate. We have measured the apparent probe size at the substrate; it remains constant in the range of 40–1000 eV. The broadening below 40 eV may explain why no large deposition yield is seen at 10 and 20 eV landing energy, despite a large abundance of electrons supposedly having the correct energy for dissociating the precursor.

Additionally regardless of the mechanism, the knowledge that the efficiency of the deposition process is greatest for a primary beam at 140 eV is directly useful for those wanting to prioritize growth speed. In addition, a primary beam of this energy has a very short penetration depth (1 nm or less), leading to minimal damage of the substrate. This technique could then be used to create EBID-deposited structures on electron-sensitive samples such biological specimens or resist.

V. CONCLUSION

In summary, electron-beam-induced deposition of platinum from methylcyclopentadienyl-platinum-trimethyl was performed with a focused beam at low landing energies down to 10 eV. The growth rate was investigated as a func-

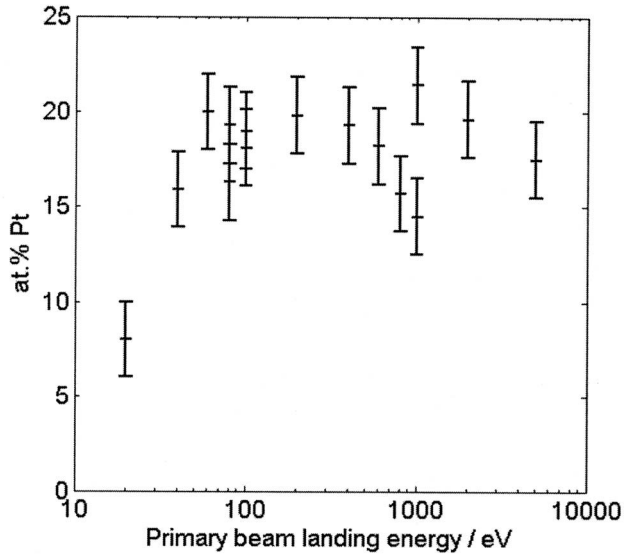

FIG. 5. Atomic concentration of platinum in the deposit as a function of beam landing energy. No significant dependence on energy was found in the range of 40–5000 eV.

tion of beam landing energy. A maximum was identified near 140 eV, where the deposition efficiency is over ten times that at 20 keV, which is consistent with expectations and literature to date. This provides further evidence for the important role of sub-20-eV secondary electrons during the dissociation process.

ACKNOWLEDGMENTS

The authors thank Harry Nulens for the AFM analysis, Peter Breimer for the EDX, and Pieter Kruit, Kees Hagen, Eric Bosch, and Frank Schuurmans for helpful discussions. This research was funded in part by an EU Marie-Curie fellowship, 6th Framework Program, No.FP6-007832-NAPS, and in part by FEI Electron Optics.

[1] S. J. Randolph, J. D. Fowlkes, and P. D. Rack, CRC Crit. Rev. Solid State Mater. Sci. **31**, 55 (2006).
[2] A. Botman, J. J. L. Mulders, R. Weemaes, and S. Mentink, Nanotechnology **17**, 3779 (2006).
[3] W. F. van Dorp, B. van Someren, C. W. Hagen, P. Kruit, and P. A. Crozier, Nano Lett. **5**, 1303 (2005).
[4] A. Broers, W. Molzen, J. Cuomo, and N. Wittels, J. Appl. Phys. **29**, 596 (1976).
[5] N. Silvis-Cividjian, C. W. Hagen, and P. Kruit, J. Appl. Phys. **98**, 084905 (2005).
[6] K. Mitsuishi, Z. Q. Liu, M. Shimojo, M. Han, and K. Furuya, Ultramicroscopy **103**, 17 (2005).
[7] D. A. Smith, Ph.D. thesis, University of Tennesse Knoxville (2007).
[8] J. D. Fowlkes, S. J. Randolph, and P. D. Rack, J. Vac. Sci. Technol. B **23**, 2825 (2005).
[9] P. D. Rack, S. Randolph, Y. Deng, J. D. Fowlkes, Y. Choi, and D. C. Joy, Appl. Phys. Lett. **82**, 2326 (2003).
[10] D. Beaulieu, Y. Ding, Z. L. Wang, and W. J. Lackey, J. Vac. Sci. Technol. B **23**, 2151 (2005).
[11] P. C. Hoyle, J. R. A. Cleaver, and H. Ahmed, J. Vac. Sci. Technol. B **14**, 662 (1996).
[12] P. C. Hoyle, J. R. A. Cleaver, and H. Ahmed, Appl. Phys. Lett. **64**, 1448 (1994).
[13] R. R. Kunz and T. M. Mayer, J. Vac. Sci. Technol. B **5**, 427 (1987).
[14] J. L. Pouchou and F. Pichoir, Rech. Aerosp. **3**, 167 (1984).
[15] T. E. Allen, R. R. Kunz, and T. M. Mayer, J. Vac. Sci. Technol. B **6**, 2057 (1988).
[16] L. Reimer, *Scanning Electron Microscopy* (Springer-Verlag, Berlin, 1985).